

1 **A morpho-tectonic approach to the study of earthquakes in Rome**

2

3 Fabrizio Marra^{1*}, Alberto Frepoli¹, Dario Gioia², Marcello Schiattarella³, Andrea
4 Tertulliani¹, Monica Bini⁴, Gaetano De Luca¹, Marco Luppichini⁵

5

6 ¹Istituto Nazionale di Geofisica e Vulcanologia, Via di Vigna Murata 605, 00143 Rome, Italy

7 ²Istituto di Scienze del Patrimonio Culturale (ISPC), Consiglio Nazionale delle Ricerche, Tito Scalo,
8 I-85050 Potenza, Italy

9 ³Dipartimento delle Culture Europee e del Mediterraneo (DiCEM), Università degli Studi della
10 Basilicata, I-75100 Matera, Italy; marcello.schiattarella@unibas.it

11 ⁴Dipartimento di Scienze della Terra, Università di Pisa, Italy

12 ⁵Dipartimento di Scienze della Terra, Università di Firenze, Italy

13

14 *corresponding author: fabrizio.marra@ingv.it

15

16 **Abstract**

17 Rome has the world's longest historical record of felt earthquakes, with more
18 than 100 events during the last 2,600 years. However, no destructive earthquake
19 has been reported in the sources and all of the greatest damage suffered in the
20 past has been attributed to far-field events. While this fact suggests that a
21 moderate seismotectonic regime characterizes the Rome area, no study has
22 provided a comprehensive explanation for the lack of strong earthquakes in the
23 region. Through the analysis of the focal mechanism and the morphostructural
24 setting of the epicentral area of a "typical" moderate earthquake (ML=3.3) that
25 recently occurred in the northern urban area of Rome, we demonstrate that this
26 event reactivated a buried segment of an ancient fault generated under both a
27 different and a stronger tectonic regime than that which is presently active. We
28 also show that the evident structural control over the drainage network in
29 this area reflects an extreme degree of fragmentation of a set of buried faults
30 generated under two competing stress fields throughout the Pleistocene. Small
31 faults and a present-day weaker tectonic regime with respect to that acting
32 during the Pleistocene might explain the lack of strong seismicity in the long
33 historical record, suggesting that a large earthquake is not likely to occur.

34

35 **Key words:** Rome; geomorphology; streambed analysis; structural geology;
36 earthquakes; seismotectonics

37

38

39

40

41

42

43

44

45

46

47 **1. Introduction**

48 On May 11th 2020, a moderate ($M_L=3.3$, $I_0=IV$ MCS) yet broadly felt earthquake
49 awoke most of the Rome's inhabitants at 05:03 a.m. (local time) (for details see
50 <https://e.hsit.it/24397691/index.html>). While producing no damage, the
51 shaking alarmed many citizens, who searched for information and reassurance
52 through the dedicated informative sources such as the INGV (Italian National
53 Institute of Geophysics and Volcanology) website. Others, instead, preferred to
54 trust on several popular beliefs which state that "Rome couldn't be struck by a
55 Big One" (i.e., a destructive earthquake with $M>7.0$), such as the mitigating effect
56 of the catacomb voids (trivial simplification from the Aristotelian theories), or
57 the protection granted by the Pope's presence. It is very likely that only few
58 people based their reactions upon a learned knowledge of the actual
59 seismotectonics features of the Rome's area. Indeed, even if a series of
60 specialized studies have been published in the last 20 years, a dedicated paper
61 investigating the reasons why Rome would not be affected by large earthquakes
62 is still missing in the scientific literature. Filling this gap is the aim of the present
63 paper in which we present a seismic study of the May 11th 2020 earthquake,
64 coupled with a statistical analysis of streambed directions in the epicentral area.
65 We identify the geometry of the seismogenic structure responsible for this $M=3.3$
66 event, and we frame it within the overall geo-morpho-structural setting of the
67 Rome's area, providing insights on the seismo-tectonic features of this region.

68

69 **2. Seismicity of the Rome's area**

70 Our knowledge on the earthquakes that affected the roman area can be resumed
 71 from the seismic catalogues' records (Guidoboni et al., 2018; Rovida et al., 2020
 72 and from the literature (e.g., Tertulliani and Riguzzi, 1995; Molin and Rossi,
 73 2004; Galli and Molin 2014; Tertulliani et al., 2020) as follows:

- 74 • very few events caused significant damage in the city (1349, 1703, 1915),
 75 according to the studies mentioned above; all these large earthquakes
 76 occurred in the Apennines mountain range;
- 77 • some other seismogenic areas surrounding Rome (e.g., the Colli Albani
 78 Volcanic District) generated events that caused moderate damage;
- 79 • the Province of Rome (hereafter GAR, is the present metropolitan area of
 80 Rome) is periodically affected by low to moderate magnitude local
 81 earthquakes which is not supposed to cause significant damage.
- 82 • Uncertain events. Catalogue records quote several earthquakes that
 83 provoked some damage in Rome (see table 1). Most of such events,
 84 occurred during the Roman Age and Early Middle Ages are poorly
 85 documented and therefore not localizable.

86 A summary of the historical and instrumental seismicity of the GAR is shown in
 87 Figure 1. Evidently, the completeness of our knowledge of seismicity decreases
 88 going back in time. In the period of ancient Rome, as well in the Early Middle
 89 Ages, strong earthquakes would seem hit Rome, sometime causing damage,
 90 whose origin is still unknown. The difficulty to understand if such earthquakes
 91 were generated by local or far-field sources depends on the documentary
 92 accounts: the earthquake was considered a prodigy, and as such, interpreted as a
 93 divine foretelling. Information on effects, damage or victims was often neglected,
 94 and very rarely documented. For these reasons we are not able to distinguish
 95 with reliability if such ancient events were originated, for example, in the
 96 Apennines region, or near Rome (in italic in table 1). In table 1 the earthquakes
 97 that hit Rome with a local intensity greater than 6 are listed.

98

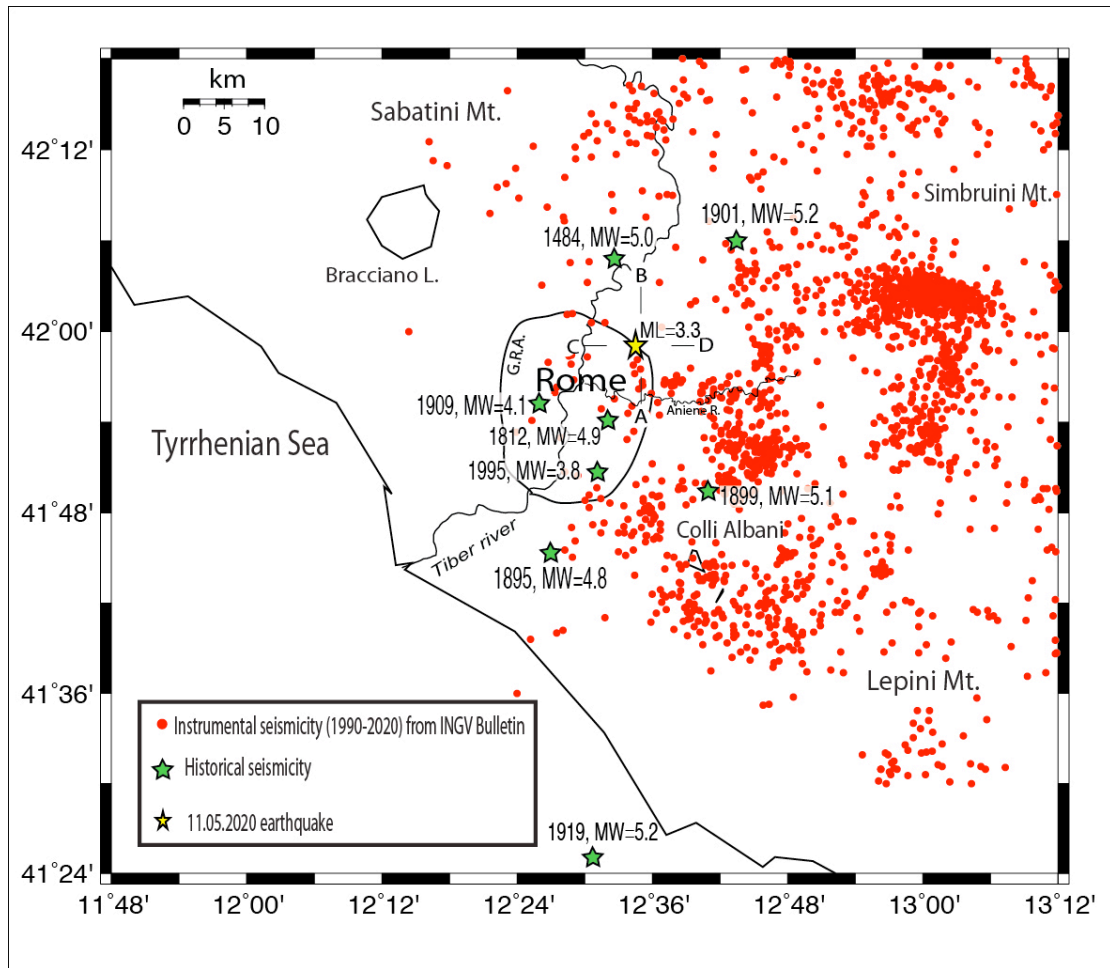
Int. in Rome	Year	Epicentral Area	Epic Int Io	Mw
<i>7-8</i>	<i>83 BC</i>	<i>Rome</i>	<i>7-8</i>	<i>5.4</i>

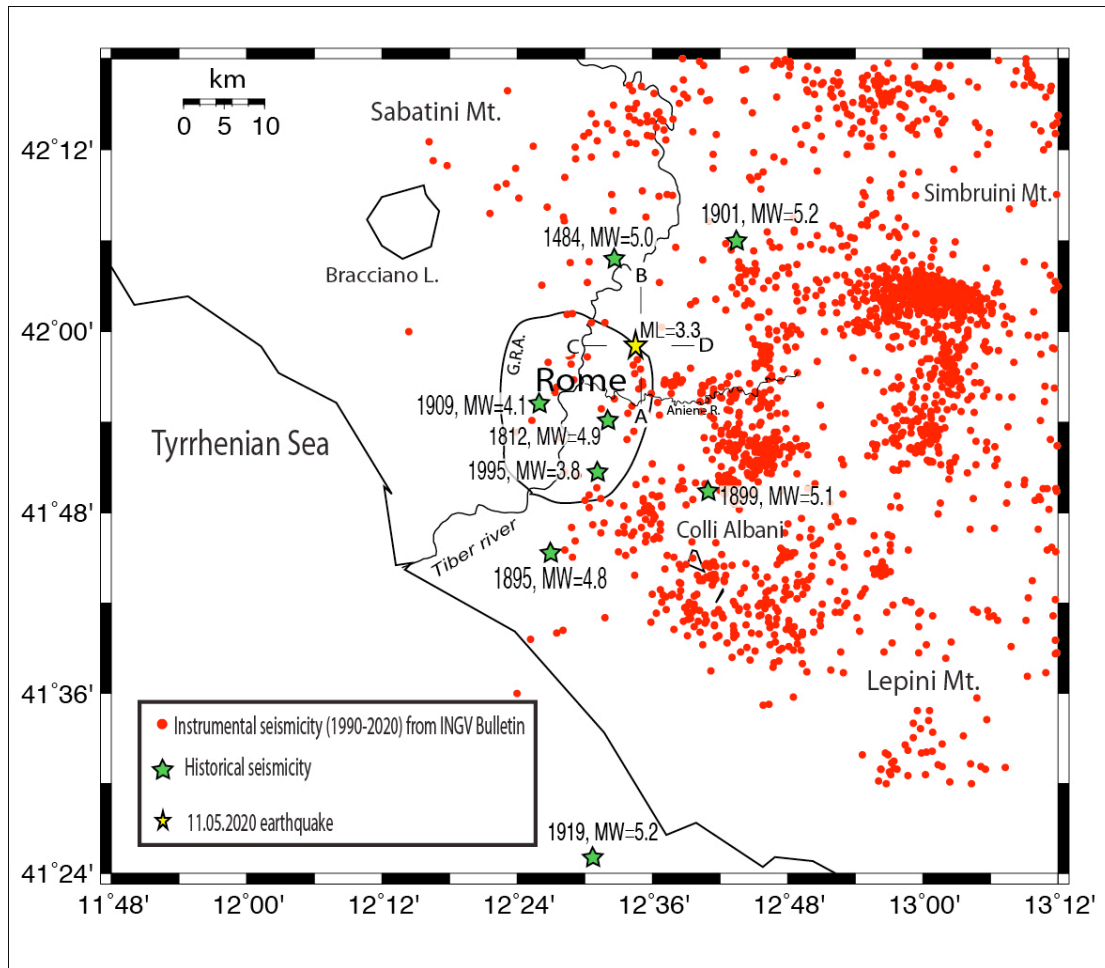
<i>7-8</i>	<i>72 BC</i>	<i>Rome</i>	<i>7-8</i>	<i>5.4</i>
<i>7-8</i>	<i>15</i>	<i>Rome</i>	<i>7-8</i>	<i>5.4</i>
<i>8</i>	<i>51</i>	<i>Rome</i>	<i>8</i>	<i>5.6</i>
<i>8</i>	<i>443</i>	<i>Rome</i>	<i>8</i>	<i>5.6</i>
<i>7-8</i>	<i>484</i>	<i>Rome</i>	<i>7-8</i>	<i>5.4</i>
<i>7-8</i>	<i>801</i>	<i>Rome</i>	<i>7-8</i>	<i>5.4</i>
<i>7</i>	<i>1091</i>	<i>Rome</i>	<i>7</i>	<i>5.1</i>
7-8	1349	Central Apennines	9	6.3
5-6	1703	Central Apennines	11	6.9
6	1703	Central Apennines	10	6.7
6	1730	Central Apennines	9	6.0
6-7	1812	Rome	6-7	4.9
5-6	1895	Rome	6-7	4.8
6-7	1899	Albani Hills	7	5.1
6-7	1915	Central Apennines	11	7.1
6	1927	Albani Hills	7	4.9

99 Table 1. List of earthquakes that caused documented damage in the present GAR.
100 The oldest events (*italic in table*) are not constrainable. (Data from Guidoboni et
101 al., 2018; Rovida et al., 2021; Tertulliani et al.; 2020).

102

103 It is interesting to note, from the seismic hazard point of view, that the epicenter
104 of several more constrainable historical events, that occurred in the Roman
105 countryside, are nowadays included in the GAR territory, densely urbanized.
106 Within this limited territory we can anyway discriminate some different clusters
107 of seismicity, in particular SE and NE of the City center. Of the first cluster are
108 part the 1812, 1895, 1995 earthquakes, while the 1901 and 2020 events are
109 located NE of the city (Figure 1). Very likely this seismicity feature is due to the
110 activity of different seismotectonic structures.





112

113 **Figure 1.** Map showing the seismicity of the Rome's area and mainshock location (blue star) of
 114 the 11.05.2020 earthquake. A-B and C-D are the cross-sections in Figure 4b. G.R.A. is the beltway
 115 around Rome.

116

117 3. Regional tectonic setting

118 In approaching the geodynamics of this region the contribution of three main
 119 mechanisms of deformation should be considered, as proposed in Faccenna et al.
 120 (1996):

121 i) the NW-SE shortening (arrow #1 in Figure 2b) induced by the convergence of
 122 Africa and Europe (Tapponier, 1977);

123 ii) the sinking of the Ionian slab (arrow #2 in Figure 2b), producing the eastward
 124 migration (arrow #3) of the Apennine arc, and consequent back-arc extension
 125 (arrow #4) in the Tyrrhenian region (Malinverno and Ryan, 1986; Patacca and
 126 Scandone, 1989);

127 iii) the gravitational spreading of the overthickened crust (arrow #5 in Figure
 128 2b) in the Apennine crustal wedge (Reutter et al., 1980; Horvath and
 129 Berckhemer, 1982).

130 All these mechanisms are to be considered presently active in the Northern
131 Apenninic arc on the basis of seismic and stress-field indications (Selvaggi and
132 Amato, 1992; Amato et al., 1993; Frepoli and Amato, 1997; Mariucci et al., 1999;
133 Lucente and Speranza, 2001; Montone and Mariucci, 2016). Moreover, crustal
134 thinning induced by extension was coupled with asthenospheric bulging (arrows
135 #6 in Figure 2b), leading to the back-arc volcanism on the Tyrrhenian margin
136 (Serri, 1997, and references therein). Such phenomena, and related magma
137 underplating, enhanced the extensional processes (arrow #6' in Figure 2b) in a
138 feedback mechanism in this region. In this regard, it is fundamental to notice that
139 the Rome area and the Alban Hills are at the southeastern margin of the Latium
140 Magmatic Province (Serri et al., 1993), and that very scanty volcanic activity
141 occurred in the area between Rome and the Ortona-Roccamonfina Line (O-R in
142 Figure 2a), which is considered (Patacca et al., 1990) a major geodynamic
143 boundary separating the Central and Southern Apennines (Figure 2a). According
144 to Marra (1999, 2001), the Sabina shear zone (Alfonsi et al., 1991) represents the
145 northern boundary of this crustal disengagement zone. Based on its proximity to
146 the Sabina shear zone, and in agreement with the numerous field evidence of
147 fault kinematics (Faccenna et al., 1994a, 1994b; Marra, 2001; Marra et al., 2004)
148 and the peculiar eruptive behaviour of the Alban Hills Volcanic District (Marra et
149 al., 2009), Frepoli et al. (2010) proposed that the transpressional stress regime
150 has been the prevailing one in this region during Quaternary times, and that it is
151 temporarily superimposed by the extensional regime during periods of incoming
152 volcanic activity and/or increased extensional activity (depending on which is to
153 be considered cause and which effect) on the Tyrrhenian margin (Figure 2b).

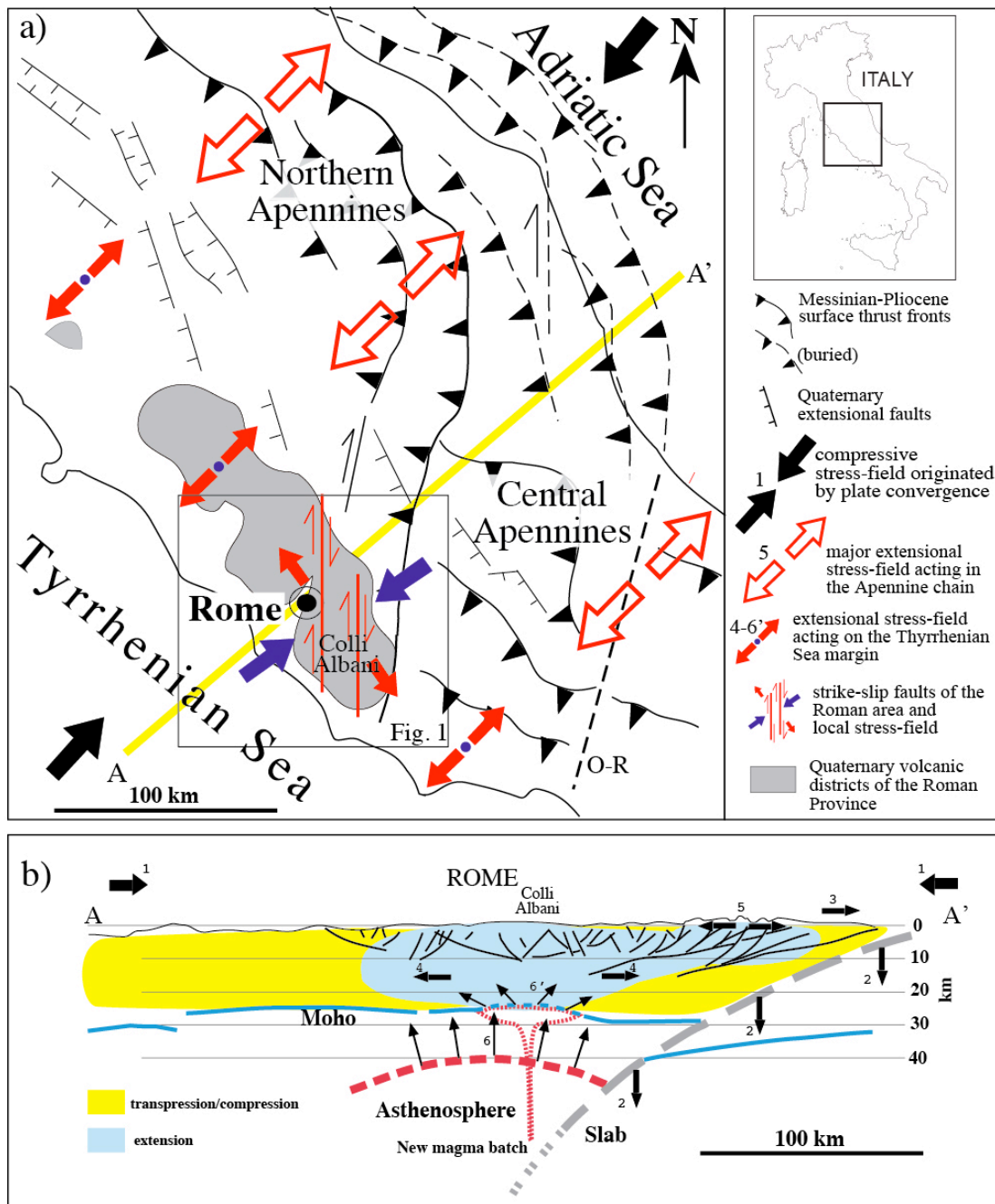
154

155

156 **4. Morpho-structural features of the Rome's area**

157 The morpho-structural setting of the Roman area originates in the deformation
158 of the geological substrate by combined faulting processes and erosion of rivers
159 and streams (Del Monte et al., 2016). Although partially obliterated by millennia
160 of anthropic interventions, it presents some evident and peculiar traits, whose
161 analysis allows us to understand the features of the tectonic forces (and related
162 stress-fields) that acted in the geological past through present time (Marra,

163 2001) (Fig. 2). Such analysis also consents to interpret the origin of the
 164 earthquakes that nowadays affect this area.
 165



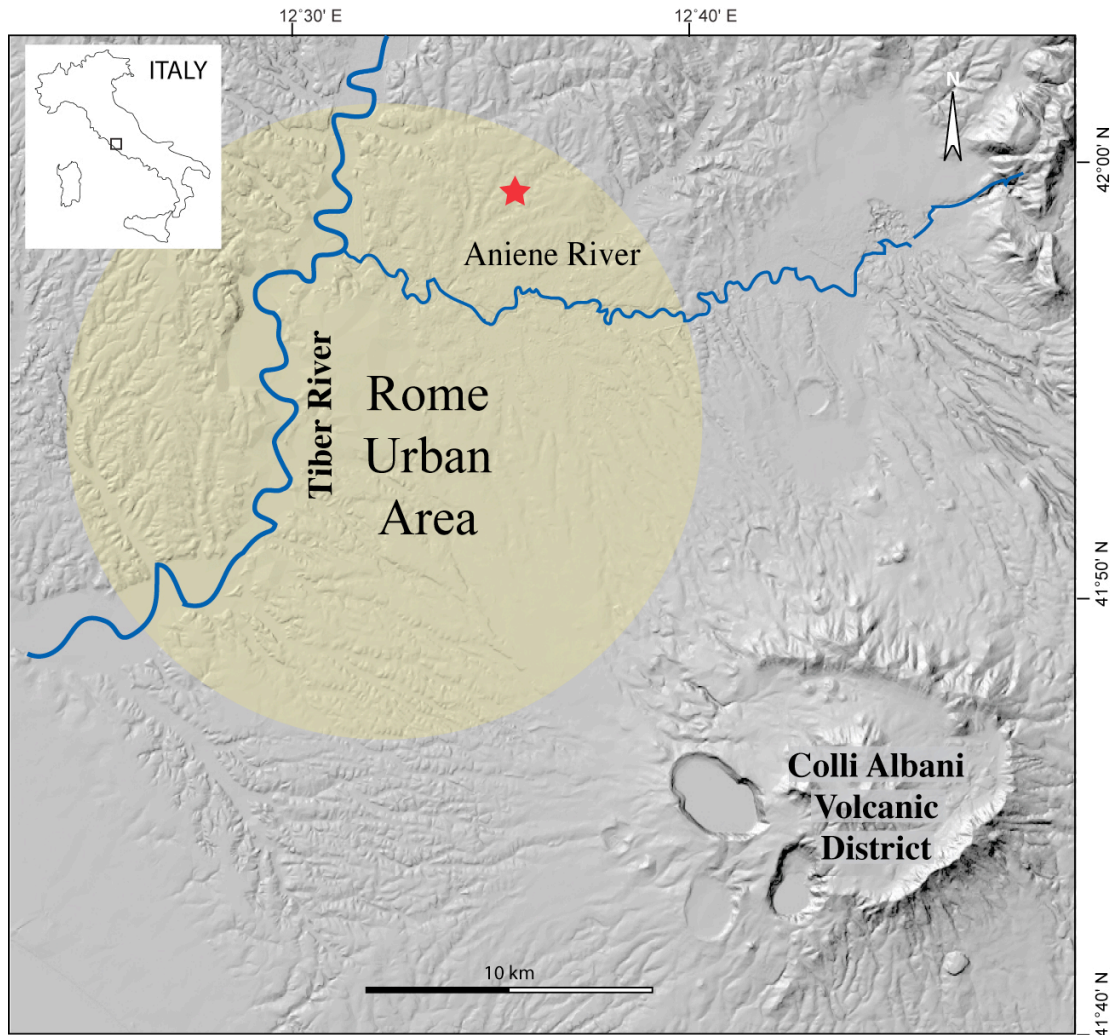
166 **Figure 2.** Structural scheme of central Italy showing the competing tectonic force fields and the
 167 main faults associated with them that acted in the Middle-Upper Pleistocene. See text for
 168 comments and explanations.
 169
 170

171

172 If we could see what the topography was like before the foundation of the City,
 173 the area of Rome would appear as a large flat sector, deeply engraved and
 174 dissected by the valleys of the tributary streams of the Tiber and Aniene Rivers,

175 and by the wider ones of the two main watercourses. While these features are
 176 less visible in the historical center of Rome, they are still well recognizable
 177 through a Digital Elevation Model (DEM) in its surrounding territory, as
 178 highlighted in Fig. 3.

179



180

181

182 **Figure 3.** Digital elevation model (DEM) of the Roman area (TINITALY by Istituto Nazionale di
 183 Geofisica e Vulcanologia (INGV), published with a CC BY 4.0 license; available at:
 184 <https://doi.org/10.13127/TINITALY/1.0>), showing the strongly marked characters of the river
 185 and stream incisions that form the hydrographic network afferent to the Tiber and the Aniene
 Rivers. Location of the 10.05.2020 earthquake is also shown (red star).

186

187

188 Most of the tabular surface highlighted by the shaded area in Fig. 3 is a
 189 "pyroclastic plateau" created by the emplacement of large coulter of volcanic
 190 deposits erupted from the Colli Albani and Monti Sabatini districts. These are
 191 represented by pyroclastic flows, originated by the collapse of the sustained
 192 eruptive column, and air-fall products such as windblown pumice, scoria and

193 lapilli. The deposition of these volcanic products, starting from around 600,000
194 years ago (Marra et al., 2014; Gaeta et al., 2016), leveled the ground creating a
195 thick, layered blanket of sediments which was soon after etched by the erosive
196 action of the watercourses. The latter, however, did not settle at random, but
197 progressively shifted in correspondence with embryonic fractures and fault lines
198 created by active tectonic deformation. The same fracturing and faulting
199 associated with the extensional tectonic regime which shaped the Tyrrhenian
200 Sea margin of central Italy during the Pleistocene allowed the magma residing in
201 the mantle to rise to the surface (e.g., Locardi et al., 1977, Acocella and Funicello,
202 2006), originating the volcanoes of the so-called "Roman Province" (Peccerillo,
203 2017) (Fig. 2). An intense seismotectonic regime must have been associated to
204 these large extensional faults, likely producing strong earthquakes throughout
205 this region.

206

207 From the end of the Middle Pleistocene (125,000 years ago), the tectonic activity
208 began to decrease in intensity, paralleling the decrease in volcanic activity
209 (Marra et al., 2004a). Hence the seismogenic potential of the faults associated
210 with this tectonic regime must also have decreased significantly. This is one of
211 the reasons why Rome is today a low seismicity area. Moderate earthquakes
212 ($M \leq 5.0$) (Tertulliani and Riguzzi, 1995; Basili et al., 1995) are almost exclusively
213 concentrated in the volcanic area of Colli Albani (Amato and Chiarabba, 1995),
214 which is in a quiescent status (Trasatti et al., 2018). The moderate seismicity of
215 the Roman area reflects an active stress-field of the same nature, but weaker,
216 than the extensive tectonic regime that characterized the Tyrrhenian Sea margin
217 of central Italy for the entire Pleistocene, as revealed by the study of the focal
218 mechanisms of these earthquakes and borehole breakouts (Montone et al., 1995;
219 Montone and Mariucci, 2016). Such weaker tectonic regime, therefore,
220 reactivates all the faults present in this region with small movements, compatible
221 with their orientation with respect to the vectors of the stress-field (Frepoli et al.,
222 2010). The seismic events associated with this regime do not generate ground
223 ruptures, as it happens for strong, heavy damaging earthquakes, because the
224 small displacements that occur on the fault planes at depth do not propagate to
225 the surface. However, these movements repeated over time generate a slow and

226 progressive deformation of the soil, conditioning the flow direction of surface
227 waters, and exerting a "structural control" on the stream axes and alluvial valleys
228 (Marra, 2001). It follows that the hydrographic network has assumed over time a
229 geometry reflecting that of the faults occurring in the geological substrate.

230

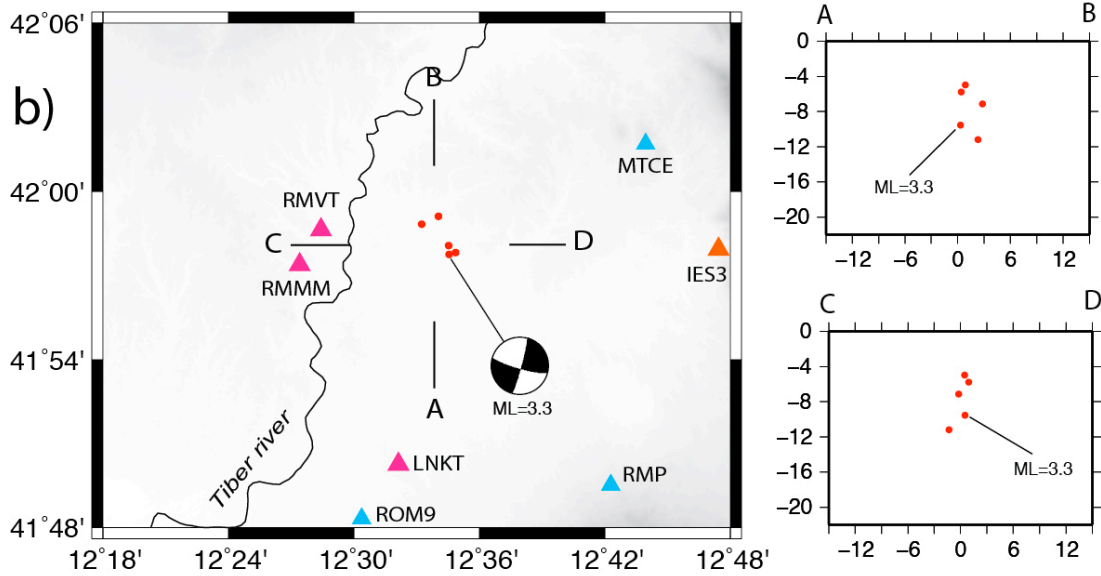
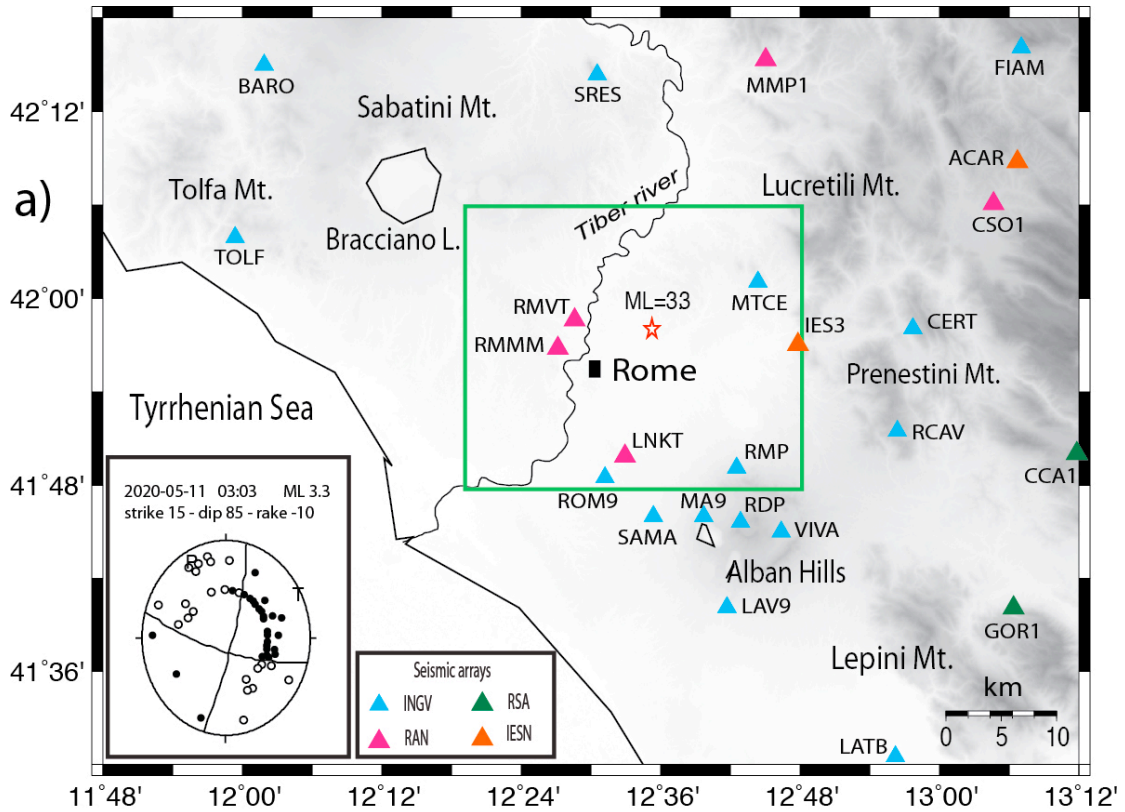
231

232 **5. Data and Methods**

233 **5.1 Seismic analysis**

234 The small seismic sequence occurred on May 11th 2020 in the north-eastern area
235 of Rome was recorded by the Italian National Seismic Network (RSN) of the
236 Istituto Nazionale di Geofisica e Vulcanologia (INGV) and by the regional seismic
237 network of Lazio and Abruzzo (RSA) (De Luca et al., 2009; Frepoli et al., 2017)
238 (Figure 4). Both national and regional Italian seismic networks have been
239 significantly extended in the last two decades through installation of new three
240 components, mostly broadband, stations. In addition we integrated the dataset of
241 this sequence with the data of the Italian strong motions network (RAN)
242 operated by the National Civil Protection Department and with the IESN network
243 (Italian Experimental Seismic Network) of Central Italy, an amateur seismic
244 network equipped with very good digitizers and sensors. This dense monitoring
245 improved in the last decade the detection and location of the seismicity in central
246 Italy.

247 To accurately relocate the seismicity, we used the Hypoellipse code (Lahr, 1989)
248 and a reliable 1D V_p velocity model computed by the application of a genetic
249 algorithm (Holland, 1975; Sambridge and Gallagher, 1993). A constant value of
250 $1.84 V_p/V_s$ determined with the Wadati method (Chatelain, 1978) was used.



251

252 **Figure 4.** a) Distribution of the seismic stations of the Italian National Seismic Network (RSN) of
 253 the Istituto Nazionale di Geofisica e Vulcanologia (INGV) and of the regional seismic network of
 254 Lazio and Abruzzo (RSA) used to locate the epicenter of the 11.05.2020 event (red star). b) Map
 255 and vertical distribution of the mainshock and two aftershocks.
 256

257 **5.2 Geomorphology**

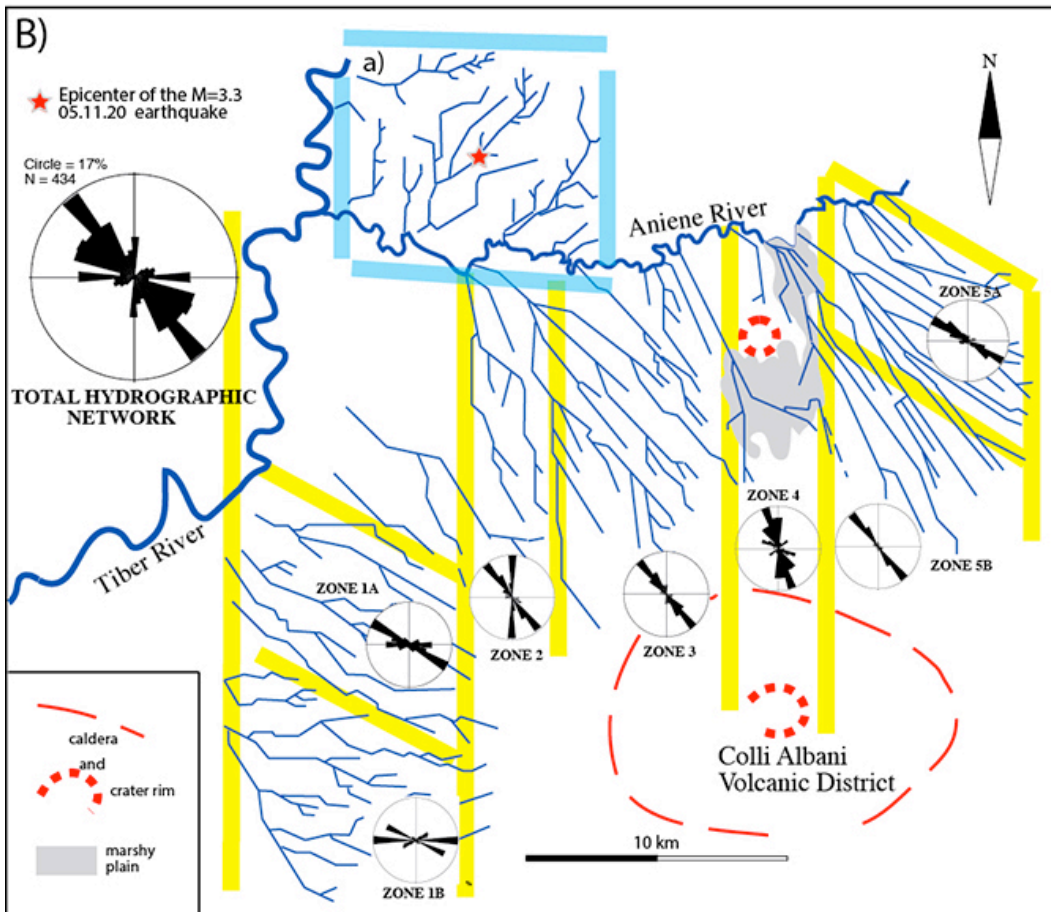
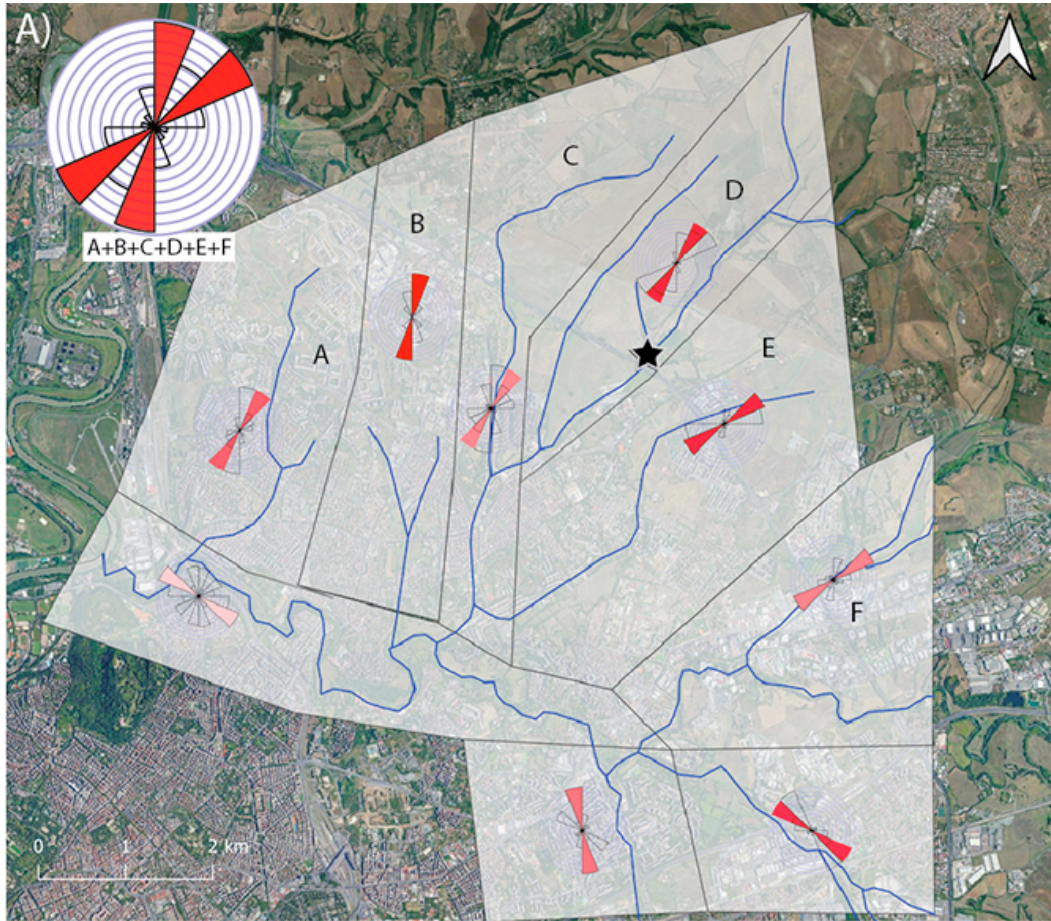
258 **5.2.1 Previous studies**

259 A quantitative analysis of drainage trends in the south-eastern area of Rome
 260 bounded by the Tiber and Aniene Rivers and by the Colli Alabani volcanic district

261 was carried out by Marra (2001). A simple technique based on statistical analysis
262 of rectified directions of streambeds was applied (e.g., Ciccacci et al., 1987;
263 Caputo et al., 1993; Macka, 2003). Stream channel directions for the total area
264 and for different sectors were weighted according to three groups of length,
265 independent of hydrographic order, and plotted on rose diagrams.

266 While it is possible that rectifying drainage patterns can introduce directionality
267 that is unrelated to structural control, it still does indicate preferential directions
268 of river flow. In the case that these preferential directions of river flow were
269 statistically significant and different from those expected from non-structural
270 controls (e.g. topographic and geographic trends), they were interpreted to be
271 diagnostic of the structural setting. Anthropogenic intervention is also possible cause
272 of rectification of water channels, however, the linearity of the alluvial valleys
273 forming in the hydrographic network consents to compare and support the
274 directionality of the streambeds. Indeed, deep incisions and a "canyon-like"
275 morphology characterizes the alluvial plains forming the hydrographic network
276 (see Fig. 3), due to the occurrence of ca. 50 m tectonic uplift in the last 250 ka
277 (Marra et al., 2016).

278



280 **Figure 5.** A) Result of the streambed direction analysis performed in this work
 281 within the hydrographic basin including the epicenter area of the May 11th event
 282 (pale-blue borders in B) is compared with that performed in the south-eastern
 283 Roman area, between the Tiber, the Aniene and the Colli Albani (B) (Marra,
 284 2001). Yellow lines border the different sectors of the analyzed drainage basins.
 285 Analysis in the historical city center was hindered by the occurrence of a
 286 widespread anthropic cover. Basemap from Qgis QuickMapServices (available
 287 under [Creative Commons Attribution-ShareAlike 3.0 licence \(CC BY-SA\)](https://plugins.qgis.org/plugins/quick_map_services/) at:
 288 https://plugins.qgis.org/plugins/quick_map_services/).

289

290 Results of the analysis conducted by Marra (2001) are shown in Fig. 5B showing
 291 that the NW-SE direction is the dominant one in the total area analysis (large
 292 diagram in the left upper corner), as opposed to an expected radial drainage
 293 trend descending from the Colli Albani caldera rim and affecting an
 294 heterogeneous geologic substrate. The maximum concentration of fluvial
 295 channel directions oriented N145° matches the strike of extension-induced faults
 296 and fractures and agrees with the present-day stress field determined from focal
 297 mechanisms and breakouts data in this region (Montone et al., 1995; Montone
 298 and Mariucci, 2016). Moreover, there are significantly different concentrations in
 299 discrete sectors delimited by the yellow lines. In particular, there are two narrow
 300 bands (zones 2 and 4) where the N-S direction of the streambeds prevails, and
 301 peculiar "domains" (zones 1A, 5A) where the WNW-ESE one is prevailing. The
 302 validation of the 'tectonic' hypothesis was performed through comparison with
 303 geometry and kinematics of fault and fractures surveyed in the area, allowing to
 304 interpret the pattern highlighted as the result of a complex structural control in
 305 this area, exerted by two competing stress-fields alternating each other
 306 throughout Pleistocene times (Marra, 1999, 2001; Frepoli et al., 2010).

307

308 **5.3 Streambed analysis**

309 In order to compare the results with previous analysis of the regional
 310 deformation pattern, a quantitative analysis of drainage trends has been
 311 performed in the discrete hydrographic basin located in the sector NE of the
 312 Tiber and Aniene Rivers confluence (Fig. 5A), within which the May 11th
 313 earthquake occurred.

314 The streambed direction analysis within the hydrographic basin including the
 315 epicenter area of the May 11th event was created by using the QGIS "Line
 316 Direction Histogram" plugin (Tveite, 2015), that visualizes the distribution of
 317 line segment directions as a rose diagram (weighted using the line segment
 318 lengths). The number of bin of direction which composes the rose diagram could

319 be set and in this work we used 8 bins corresponding to the main cardinal
320 directions. The tiles in which the area has been divided were identified
321 according to the main directions of streambeds.

322

323 **5.4 Drainage network anomalies and river profile analysis**

324 Drainage network anomalies are one of the most useful morphotectonic
325 indicators of active tectonics and they are widely used as an effective tool to infer
326 the possible control of fault activity on landscape and channels (see for example,
327 Boulton et al., 2014; Calzolari et al., 2016; Pavano et al., 2016; Kent et al., 2017;
328 Baharami, 2013). Integrated studies of possible active tectonic control on the
329 geometry of the drainage network frequently include analysis of river
330 longitudinal profiles, preferential orientation and alignments of channels, right-
331 angle confluences and fluvial elbows (Boulton et al., 2014; Pavano et al., 2016;
332 Kent et al., 2017; Gioia et al., 2018). Indeed, river profile analysis is one of the
333 most powerful tools for the identification of transient state of a drainage
334 network and recognition of knickpoints/knickzones, which represent valuable
335 and effective morphotectonic markers of recent crustal deformation (Whipple
336 and Tucker, 1999). Our approach combines the analysis of anomalies in drainage
337 network geometry (i.e. preferential orientation and/or alignments of channels,
338 fluvial elbows, right-angle confluences) with the identification of
339 knickpoints/knickzones of tectonic origin in transient longitudinal river profiles.
340 Such data have been used as morphotectonic evidences of active/recent tectonic
341 deformation induced by fault system responsible for the seismic activity of the
342 study area.

343 River profile analysis has been carried out according to the methods and
344 procedures developed by Wobus et al. (2006), Forte and Whipple (2019) using a
345 DEM with a spatial resolution of 10 m. Stream profile analysis is classically
346 carried out by identifying knickpoints or knickzones along the river longitudinal
347 profiles or by extracting a linear regression in a log-log slope-area graph, which
348 allowed us to extrapolate the concavity index (the slope of the regression) and
349 the steepness index (the y-intercept, that is the projection of the best-fit line that
350 intersects the y-axis). Knickpoints or abrupt scarps of the longitudinal profiles
351 can be related to tectonic- or eustatic- induced perturbations of ancient base-

352 levels but their formation and migration can be also related to a co-seismic fault
353 ruptures or deformation induced by blind faults (Kirby and Whipple, 2012). In
354 particular, the identification of fault-induced disturbance on channel profiles can
355 be performed through the recognition of linear alignments of
356 knickpoints/knickzones in channels with different sizes and orientations
357 (Boulton et al., 2014; Kirby and Whipple, 2012).
358 In order to investigate the possible occurrence of fault-related knickpoints and
359 river profile anomalies, we have investigated the river longitudinal profiles of the
360 main channels of the study area through the identification and mapping of
361 abrupt changes in river profile shape. Such data have been combined with the
362 morphotectonic analysis of the spatial distribution of drainage network
363 anomalies. Then, their spatial distribution has been used to infer the traces of
364 possible tectonic lineaments of the study area.

365

366 **6. Results**

367 **6.1 Focal mechanism and re-location of the 11 May earthquake**

368 The M_L 3.3 mainshock (11 May at 03:03 UTC) was followed over the next two
369 days by only four small aftershocks with magnitude ranging from 0.7 to 1.8
370 (Table 2). Thanks to the high station coverage we were able to determine all
371 earthquake hypocenter depths with acceptable uncertainties. The average
372 location errors are 0.14 km (horizontally) and 0.32 km (vertically) with a
373 confidence level of 90%. Mainshock hypocenter is at 9.6 km of depth, while the
374 aftershock hypocenters are ranging from 5.0 to 11.2 km of depth (Fig. 4). The
375 two largest aftershocks (magnitude M_L 1.8 and 1.4, respectively) have depth
376 between 5.0 and 5.8 km, and are located very close to the mainshock epicenter,
377 while the two smallest aftershocks (both magnitude M_L 0.7) are located slightly
378 towards NW with respect to the mainshock epicenter, at 7.2 and 11.2 km of
379 depth. These two aftershocks are clearly unrelated with the seismogenic
380 structure responsible for the mainshock and are likely the effect of stress
381 propagation to a contiguous fault.

382

383

384

385

386

387 Table 2. List and localization parameters of the Rome sequence (May 2020).

388

389

Date	Origin time	Lat	Lon	Depth	Azimuthal gap	RMS	Magnitude M_L
2020-05-11	03:03	41 57.77	12 34.54	9.6	44	0.14	3.3
2020-05-11	03:14.43	41 59.13	12 34.05	7.2	72	0.12	0.7
2020-05-11	03:14.47	41 58.84	12 33.25	11.2	73	0.11	0.7
2020-05-12	00:06	41 57.83	12 34.87	5.8	47	0.18	1.8
2020-05-13	00:07	41 58.08	12 34.53	5.0	46	0.20	1.4

390

391 We have computed the fault plane solution of the mainshock with the FPFIT code

392 (Reasenbergs and Oppenheimer, 1985). First-motion polarities are 57. The focal

393 mechanism has a large strike-slip component (first nodal plane: strike 15, dip 85,

394 rake -10). T-axis is oriented in a NE-SW direction according with the general

395 "Antiapennine" (NE-SW) extension. Following some tectonic information of this

396 area, the fault plane coincides with the NNE-SSW nodal plane of the solution

397 which has a left-lateral strike-slip kinematics.

398

399 **6.2 Statistical analysis of streambed directions in the epicenter area**

400 Results of the streambed analysis in the small hydrographic basin where the

401 epicenter of the May 11th earthquake occurred are summarized in Fig. 5A.

402 The streambeds in the eastern portion of the basin (discrete sectors D, E, F)

403 concentrate around the NE-SW direction, which is the one expected based on the

404 topographic gradient, perpendicular to the Aniene River course, towards which

405 the catchment basin drains. In contrast, an abrupt rotation occurs in the western

406 portion of the basin (discrete sectors A, B, C), where the streambeds are aligned

407 along the NNE-SSW direction, parallel to the main watercourse of the Tiber

408 River. Similarly to the results obtained in the southern area by Marra (2001),

409 showing that the ca. N-S direction is a characteristic feature of the streambeds in

410 this region which is clearly independent by the geographic and topographic

411 control on the hydrographic network, we interpret the N-S lineaments to reflect

412 tectonic control on the streambeds exerted by fault activity in the analyzed basin.

413 As it has been remarked in previous works (e.g., Alfonsi et al., 1991; Faccenna et

414 al., 1994, 2008; Marra et al., 2004b) strike-slip, right-lateral N-S faults have been

415 active repeatedly during the Pleistocene, up to historical times. Frepoli et al.

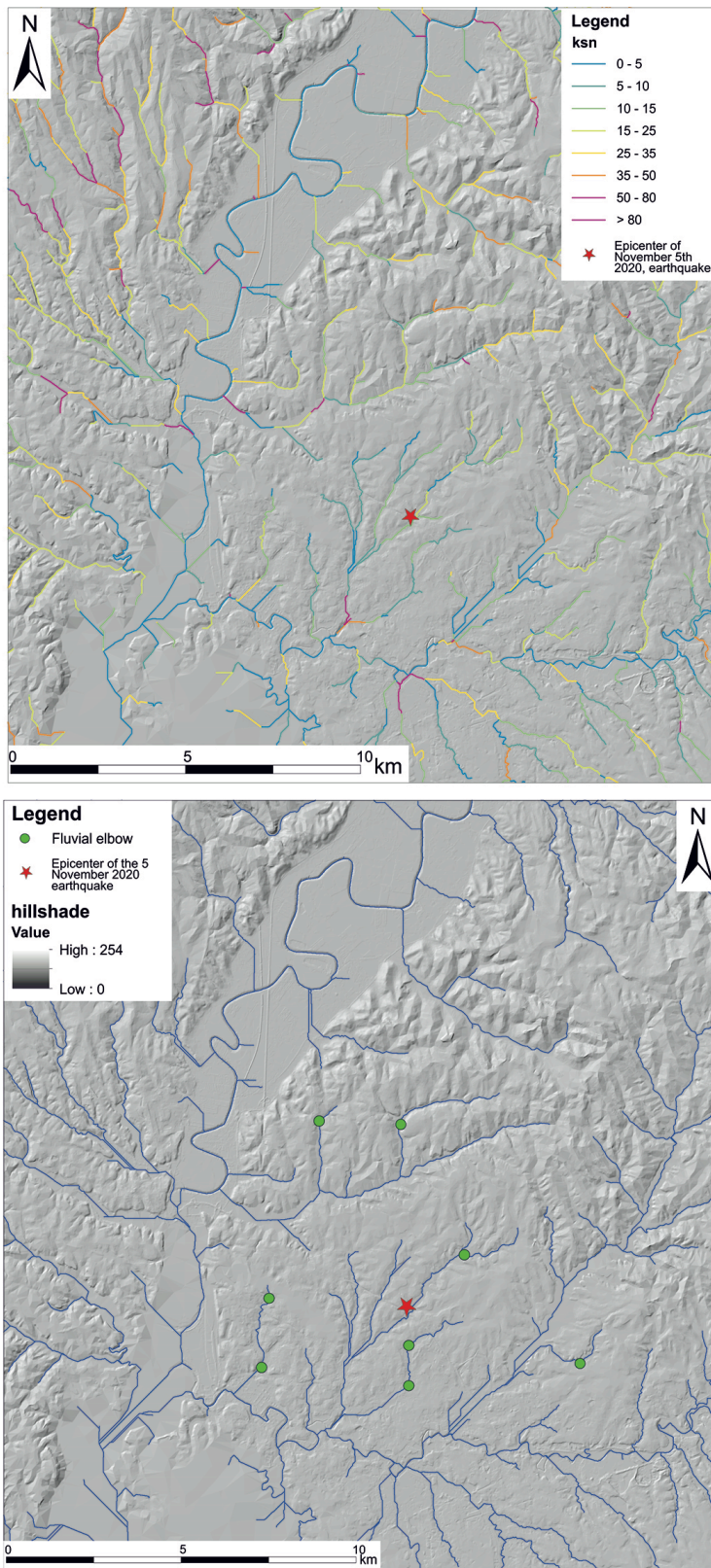
416 (2010) have remarked on the direct relationship between the sectors
417 characterized by N-S direction of the streambeds and seismically active fault
418 zones. It is worth noting that the May 11th earthquake epicenter occurs on the
419 northern continuation of one such N-S zone (zone 2 in Fig. 5B).

420

421 **6.3 Morphotectonic analysis of the drainage network: river profile analysis** 422 **and drainage network anomalies**

423 Analysis of longitudinal river profiles of the bedrock-rivers is based on the
424 stream power incision model (Whipple and Tucker, 1999; Wobus et al., 2006;
425 Forte and Whipple, 2019) and has been carried out to evaluate the channel
426 response to eustatic- and tectonic-induced processes. In a first step, we prepare a
427 map of the normalized steepness index (ksn) with a reference concavity index of
428 $\theta_{ref} = 0.45$ (Fig. 6a). Ksn map allowed us to perform a preliminary analysis of the
429 spatial distribution of ksn values, which can be useful to individuate the sectors
430 of the landscape featured by knickpoints and knickzones of tectonic origin.
431 Moreover, a morphotectonic map showing the spatial distribution of fluvial
432 elbows and anomalies in drainage network geometry was also introduced (Fig.
433 6b). Fig. 7 shows the results of the analysis of the river profiles, which highlights
434 how most of the channels deviates from the typical equilibrium shape of the
435 longitudinal profiles. Longitudinal profiles are featured by the presence of
436 knickpoints and knickzones, mainly in the central reach of the river profiles.
437 These knickpoints appear not controlled by lithological contact and suggest a
438 transient state of the fluvial net induced by tectonic perturbation or eustatic
439 base-level variations. In particular, we detect the occurrence of convex zones or
440 knickpoints related to a past base-levels, as testified by the presence of a large
441 “terraced surfaces” at altitude ranging from 60 to 40 m a.s.l. (Fig. 7). Our analysis
442 also reveals the occurrence of a cluster of knickpoints in the right-orographic
443 side of the Aniene River with different features than the previous ones. In fact,
444 they can be classified as slope-break knickpoint (*sensu* Wobus et al., 2006, see
445 also Kirby and Whipple, 2012) and are aligned along NW-SE and N-S orientation.
446 Such alignments as well as the location of anomalous confluences and right-angle
447 elbows of the drainage network allowed us to infer the occurrence of the tectonic

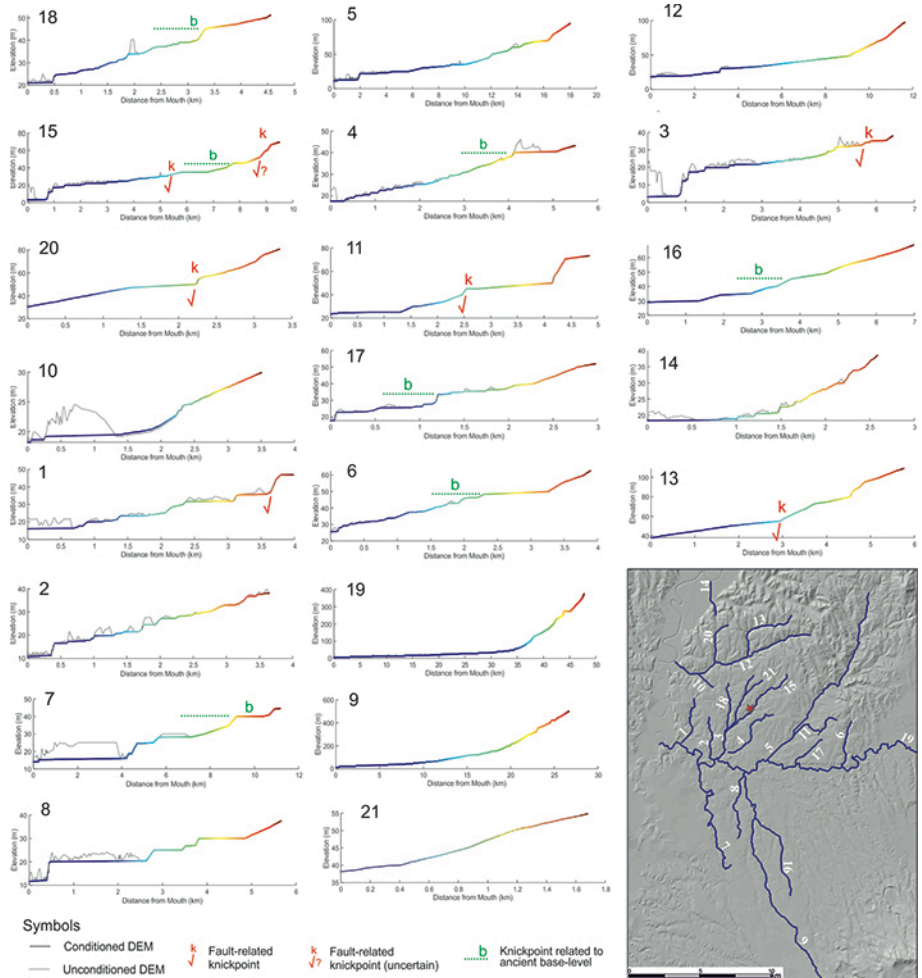
448 lineaments mapped in Fig. 8, which can be responsible for the recent tectonic
 449 activity that promoted the perturbation of the fluvial net.



450

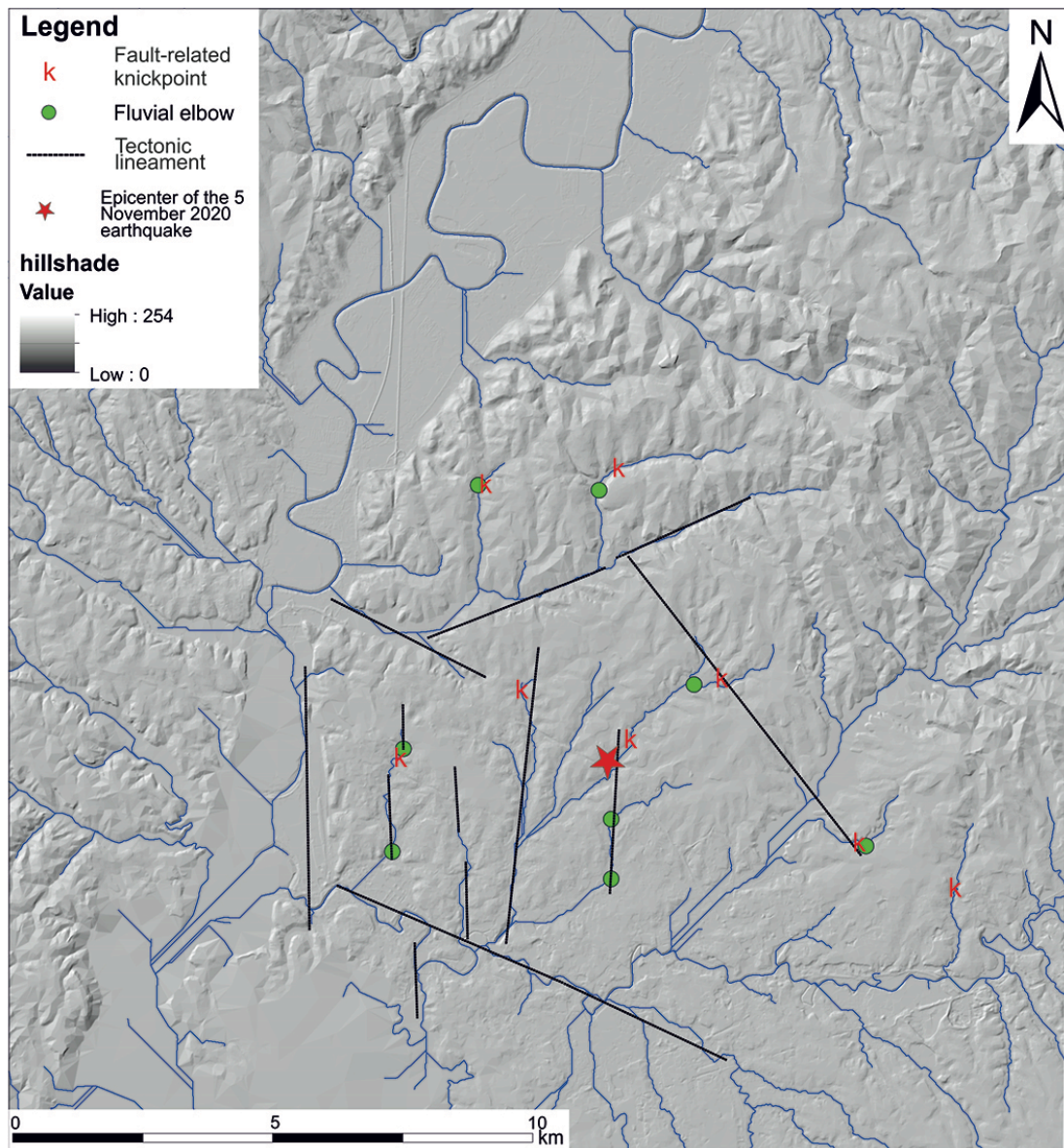
451 **Figure 6.** a) Hillshade of the study area and distribution of the normalized channel steepness
 452 index (ksn, $\theta_{ref} = 0.45$); b) Drainage network of the study area and main planar anomalies of the
 453 fluvial net. Tectonic lineaments inferred by morphotectonic analysis are also showed.

454



455
456
457
458

Figure 7. Longitudinal profiles of the main channels of the study area (location and numbering in the main map) and interpretation of the knickpoints.



459
460 **Figure 8.** Tectonic lineaments of the study area inferred by morphotectonic analyses and the
461 spatial distribution of the main drainage network anomalies of the study area (i.e. fluvial elbow
462 and knickpoints of river profiles). Hillshade was derived by the 10 m TINITALY DEM, published
463 with a CC BY 4.0 license by Istituto Nazionale di Geofisica e Vulcanologia (INGV), available at:
464 <https://doi.org/10.13127/TINITALY/1.0>.
465

466
467
468

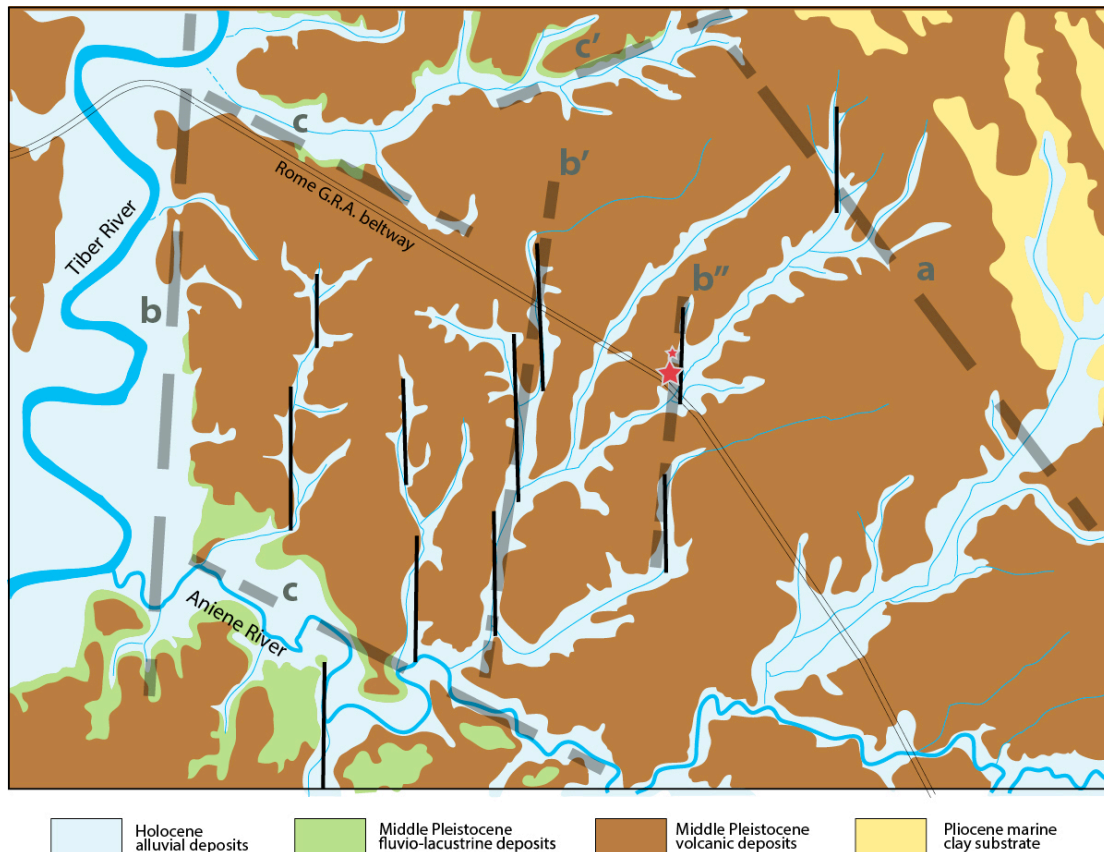
469 **7. Discussion**

470 Studies conducted during the last two decades on the geological-structural and
471 seismic-tectonic setting of the Roman area have shown that the geometry of the
472 hydrographic network reflects that of a set of buried faults (Marra, 199, 2001;
473 Frepoli et al., 2010). Considering the significant offsets affecting the Middle-
474 Pleistocene volcanic deposits in this area (e.g., Faccenna et al., 1994a, 1994b;
475 Marra, 2001) compared to the lack of strong events in the historical record, it is

476 inferred that these faults are no longer active with the seismic intensity they had
477 in the geological past. We conclude that they are reactivated under the effect of
478 the stress-field that currently acts in the upper crust and determines the genesis
479 of low-magnitude earthquakes in this region.

480 In particular, it has been shown that the drainage network pattern and the
481 distribution of river profile anomalies (i.e. fluvial elbows and
482 knickpoint/knickzones) reflect the deformation field induced on the surface by
483 the reactivation of these buried faults, with a set of three preferential alignments:
484 i- The first displays an NW-SE "Apennine" direction, ("a" in Fig. 9), which
485 precisely reflects that of the large, dip-slip extensional faults that first created the
486 Tyrrhenian Sea marine basins (Barberi et al., 1994) and later, in the lower-
487 middle Pleistocene, the so-called "Tyrrhenian margin" (Fig. 2). This is a wide
488 hilly or sub-flat area between the Apennine chain and the present coast,
489 originated by the fault displacement and the "staircase" lowering of the
490 mountain relief (Parotto and Praturlon, 1975). The direction of these faults also
491 reflects the alignment of the volcanoes that developed in the Middle Pleistocene
492 along the Tyrrhenian margin, following the rise of magmas mainly along the
493 fractures in the earth's crust created by these tectonic structures (Locardi et al.,
494 1977).

495



496
497
498
499
500
501
502
503
504
505
506
507

Figure 89. Geo-morpho-structural setting of the epicenter area. The thicker dashed lines represent the main buried faults inferred from the analysis of the hydrographic network, with the exception of the "a" fault, interpreted on the basis of the presence of a structural high to the NE, represented by outcrops of Pliocene sediments. A fourth set of NE-SW lineaments is likely originated by the topographic gradient in this area and is not highlighted as potential structural control. The thin, solid lines represent the superficial expression of the deformation linked to faults that are continuous at depth (b', b''), evidenced by straight tracts of the riverbeds. One of these deep NNE-SSW faults is the one that generated the May 11th earthquake, as the focal mechanism of this event suggests.

508

509 ii- The second set of lineaments has a direction from NS to NNE-SSW ("b" in Fig.
510 9) and reflects that of even older faults, with right-lateral strike-slip character
511 (i.e. sub-vertical faults with right-hand horizontal movement (Alfonsi et al., 1991;
512 Faccenna et al., 1994). These faults are linked to the dismemberment of the
513 Apennine chain in independent arcs, due to the fragmentation of the "slab", that
514 is the "Adriatic" tectonic plate which subducted below the Apennine orogenic
515 chain (Malinverno and Rayan, 1986; Patacca et al., 1990). However, these faults
516 have been active until recent times (Faccenna et al., 2008; Marra et al., 2004b),
517 probably due to the independent geodynamic mechanism that generated them,
518 and are competing with the regime of forces that originated the extensional

519 faults (Marra, 2001; Faccenna et al., 1996). We also know from the analysis of the
520 focal mechanisms of local earthquakes that small N-S fault segments are
521 currently reactivated with opposite movement (left-lateral) together with the
522 "Apennine", dip-slip faults (Frepoli et al., 2010).

523

524 iii- Finally, a third set of lineaments has conjugated WNW-ESE and ENE-WSW
525 directions ("c" and "c'" in Fig.9) and creates particular rhomboid "domains"⁹.
526 Within these discrete regions, the N-S direction (as in the case of the epicenter
527 area of the Rome's May 11th, 2020 earthquake, Fig. 9), or the same WNW-ESE
528 directions (sectors 1A and 5A in Fig. 5B) may prevail. The origin of these
529 domains is linked to the strike-slip faults and can be generated between two
530 long, parallel N-S lineaments (Jones and Tanner, 1995). The characteristic of the
531 strike-slip (transcurrent) faults is precisely that of being arranged in parallel
532 with "en-echelon" geometry, that is, along stairway segments which can,
533 however, locally have a lateral overlap between them (Sylvester, 1988). The en-
534 echelon geometry characterizes the surface expression of faults that are
535 continuous at depth (Sylvester, 1988) (examples b' and b" in Fig. 9).

536

537 **8. Conclusions**

538 The analysis of the hydrographic network in the epicenter area of the May 11th,
539 2020 earthquake shows a relative maximum concentration of the streambed in
540 the NNE-SSW direction: some of such rectilinear tracts, arranged with en-
541 echelon geometry, are highlighted in Fig. 5. We interpret these features as the
542 surface expression of buried NNE-SSW, strike-slip faults. Indeed, the focal
543 mechanism and aftershock alignment reveal that one of these buried ~N-S fault
544 reactivated with left-lateral movement on the occasion of the May 11th 2020
545 earthquake. Effectively, tectonically sensitive geomorphic analyses revealed the
546 occurrence of a cluster of knickpoints in the right side of the Aniene River that
547 can be classified as slope-break knickpoints and are aligned along NW-SO and N-
548 S orientation. Such a fluvial net perturbation corroborates the hypothesis of
549 recent tectonic activity affecting the study area along those faults.

550 When we consider the multitude of lineaments that are present at a wider and at
551 a smaller scale in this region (e.g., Fig. 2 and Fig. 9, respectively), we realize the

552 extreme fragmentation deriving from the intricate network of genetically
553 different faults. Such fragmentation results into a number of small fault
554 segments, with respect to the original long fault lines generated under the
555 competitive tectonic regimes that affected this region during Pleistocene times.
556 We remark that such high fragmentation is mainly provided by a en-echelon
557 system of ~N-S strike-slip faults which have crustal continuity. Therefore
558 hindering the lateral continuity of the NW-SE trending faults, which represent
559 the most favorably oriented fault system with respect to the Present-day NE-SW
560 extensional regime.
561 Small fault planes and a weaker tectonic regime explain the occurrence of
562 moderate seismicity and provide a likely explanation for the inhabitants of Rome
563 of the reason why they should not expect that a large earthquake may affect the
564 City.

565

566

567 Additional information

568 The authors declare no competing financial and non-financial interests.

569

570 Data availability statement

571 All data generated or analyzed during this study are included in this published
572 article.

573

574 Author Contribution statement

575

576 F.M. conceptualization, methodology, validation, investigation, Writing - Original
577 draft, supervision

578 A.F. methodology, validation, investigation, data curation, Writing - Original draft

579 D.G. methodology, validation, investigation, data curation, Writing - Original draft

580 M.S. methodology, validation, investigation, data curation, Writing - Original

581 draft

582 A.T. methodology, validation, investigation, data curation, Writing - Original draft

583 M.B. methodology, validation, investigation, data curation, Writing - Review and
584 editing

585 G.D.L. methodology, validation, investigation, data curation, Writing - Review and
586 editing

587 M.L. methodology, validation, investigation, data curation, Writing - Review and
588 editing

589

590

591

592

593

594

595

596 REFERENCES

597

598 Acocella, V., & Funiciello, R. (2006). Transverse systems along the extensional
599 Tyrrhenian margin of central Italy and their influence on volcanism. *Tectonics*,
600 25(2), TC2003.

601

602 Alfonsi, L., Funiciello, R., Mattei, M., Girotti, O., Maiorani, A., Preite Martinez, M.,
603 Trudu, C., Turi, B.: Structural and geochemical features of the Sabina strike-slip
604 fault (Central Apennines), *Bollettino della Società Geologica Italiana*, 110, 217-
605 230, 1991.

606

607 Amato, A., B. Alessandrini, G.B. Cimini, A. Frepoli, and G. Selvaggi, Active and
608 remnant subducted slabs beneath Italy: evidence from seismic tomography and
609 seismicity, *Ann. Geofis.*, 36 (2), 201-214, 1993.

610

611 Amato, A. and Chiarabba, C.: Earthquake occurrence and crustal structure, in:
612 *The Volcano of the Alban Hills*, edited by Trigila, R., Univ. degli Studi di Roma "La
613 Sapienza", Rome, 193–211, 1995.

614

615 Bahrami, S.: Analyzing the drainage system anomaly of zagros basins:
616 Implications for active tectonics, *Tectonophysics*, 608, 914-28, 2013.

617

618 Barberi, F., Buonasorte, G., Cioni, R., Fiordelisi, A., Foresi, L., Iaccarino, S.,
619 Laurenzi M.A., Sbrana, A., Vernia, L., Villa, I.M.: Plio-Pleistocene geological
620 evolution of the geothermal area of Tuscany and Latium, *Mem. Descr. Carta Geol.*
621 *Ital.*, 49, 77-134, 1994.

622

623 Basili, A., Cantore, L., Cocco, M., Frepoli, A., Margheriti, L., Nostro, C., Selvaggi, G.:
624 The June 12, 1995 microearthquake sequence in the city of Rome, *Ann. Geofis.*,
625 39(6), 1167–1175, 1996.

626

627 Boulton, S.J., Stokes, M., Mather, A.E.: Transient fluvial incision as an indicator of
628 active faulting and Plio-Quaternary uplift of the Moroccan High Atlas,
629 *Tectonophysics*, 633, 16-33, doi: 10.1016/j.tecto.2014.06.032, 2014.

630

631 Calzolari, G., Della Seta, M., Rossetti, F., Nozaem, R., Vignaroli, G., Cosentino, D.,
632 Faccenna, F.: Geomorphic signal of active faulting at the northern edge of Lut
633 Block: Insights on the kinematic scenario of Central Iran, *Tectonics*, 35(1), 76-
634 102, doi: <https://doi.org/10.1002/2015TC003869>2016.

635

636 Caputo, C., Ciccacci, S., De Rita, D., Fredi, P., Lupia Palmieri, E., Salvini, F.: Drainage
637 pattern and tectonics in some volcanic areas of Latium (Italy), *Geologica Romana*,
638 29, 1-13, 1993.

639

640 Chatelain, J.L.: Etude fine de la sismicité en zone de collision continentale à l'aide
641 d'un réseau de stations portables: la region Hindu-Kush-Pamir. Thèse de 3^{ème}
642 cycle, Univ. Paul Sabatier, Toulouse, 1978.

643

- 644 Ciccacci, S., Fredi, P., Lupia Palmieri, E., Salvini, F.: An approach to the
645 quantitative analysis of the relations between drainage pattern and fracture
646 trend, in: *International Geomorphology 1986*, edited by Gardiner, V., Proceedings
647 of the First International Conference on Geomorphology, Part II, John Wiley and
648 Sons Ltd, Chichester, 49-68, 1987.
- 649
650 Del Monte, M., D'Orefice, M., Luberti, G.M., Marini, R., Pica, A., Vergari, F.:
651 Geomorphological classification of urban landscapes: the case study of Rome
652 (Italy), *Journal of Maps*, 12, 178-189, DOI:10.1080/17445647.2016.1187977,
653 2016.
- 654
655 De Luca, G., Cattaneo, M., Monachesi, G., Amato, A.: Seismicity in central and
656 northern Apennines integrating the Italian national and regional networks,
657 *Tectonophysics*, 476(1), 121-135, doi:10.1016/j.tecto.2008.11, 2009.
- 658
659 Faccenna, C., Funiciello, R., Mattei, M.: Late Pleistocene N-S shear zones along the
660 Latium Tyrrhenian margin: structural characters and volcanological
661 implications, *Bollettino di Geofisica Teorica Applicata*, 36, 507-522, 1994a.
- 662
663 Faccenna, C., R. Funiciello, P. Montone, M. Parotto, and M. Voltaggio, An example
664 of late Pleistocene strike-slip tectonics: the Acque Albule basin (Tivoli, Latium),
665 *Mem. Descr. d. Carta Geol. d'It.*, 49, 37-50, 1994b.
- 666
667 Faccenna, C., Davy, P., Brun, J.P., Funiciello, R., Giardini, D., Mattei, M., Nalpas, T.:
668 The dynamics of back-arc extension: an experimental approach to the opening
669 of the Tyrrhenian Sea, *Geophysical Journal International*, 126, 781-795, 1996.
- 670
671 Faccenna, C., Soligo, M., Billi, A., De Filippis, L., Funiciello, R., Rossetti, C.,
672 Tuccimei, P.: Late Pleistocene depositional cycles of the Lapis Tiburtinus
673 travertine (Tivoli, Central Italy): Possible influence of climate and fault activity,
674 *Global and Planetary Change*, 63(4), 299-308, 2008.
675 doi:10.1016/j.gloplacha.2008.06.006
- 676
677 Forte, A.M. and Whipple, K.X.: Short communication: The Topographic Analysis
678 Kit (TAK) for TopoToolbox, *Earth Surf Dynam*, 7(1), 87-95, doi: 10.5194/esurf-7-
679 87-2019, 2019.
- 680
681 Frepoli, A., and A. Amato, Contemporaneous extension and compression in the
682 northern Apennines from earthquake fault-plane solutions, *Geophys. J. Int.*, 129,
683 368-388, 1997.
- 684
685 Frepoli A, Marra F, Maggi C, Marchetti A, Nardi A, Pagliuca NM, et al. Seismicity,
686 seismogenic structures and crustal stress field in the greater area of Rome
687 (Central Italy). *Journal Geophysical Research* 2010;115.
688 doi:10.1029/2009JB006322, 2010
- 689
690 Frepoli, A., Cimini, G.B., De Gori, P., De Luca, G., Marchetti, A., Monna, S., Montuori,
691 C., Pagliuca, N.: Seismic sequences and swarms in the Latium-Abruzzo-Molise
692 Apennines (central Italy): new observations and analysis from a dense

- 693 monitoring of the recent activity, *Tectonophysics*, 712-713, 312-329,
694 doi.org/10.1016/j.tecto.2017.05.026, 2017.
- 695
- 696 Galli, P.A.C. and Molin, D.: Beyond the damage threshold: the historic
697 earthquakes of Rome, *Bull Earthquake Eng.*, 12, 1277–1306,
698 <https://doi.org/10.1007/s10518-012-9409-0>, 2014.
- 699
- 700 Gaeta, M., Freda, C., Marra, F., Arienzo, I., Gozzi, F., Jicha, B., Di Rocco, T.: Paleozoic
701 metasomatism at the origin of Mediterranean ultrapotassic magmas: constraints
702 from time-dependent geochemistry of Colli Albani volcanic products (Central
703 Italy), *Lithos*, 244, 151-164, 2016.
- 704
- 705 Gioia, D., Schiattarella, M., Giano, S.: Right-Angle Pattern of Minor Fluvial
706 Networks from the Ionian Terraced Belt, Southern Italy: Passive Structural
707 Control or Foreland Bending?, *Geosciences*, 8(9), 331, PubMed PMID,
708 [doi:10.3390/geosciences8090331](https://doi.org/10.3390/geosciences8090331), 2018.
- 709
- 710 Guidoboni, E., Ferrari, G., Mariotti, D., Comastri, A., Tarabusi, G., Sgattoni, G.,
711 Valensise, G.: CFTI5Med, Catalogo dei Forti Terremoti in Italia (461 a.C.-
712 1997) e nell'area Mediterranea (760 a.C.-1500), Istituto Nazionale di Geofisica
713 e Vulcanologia (INGV), <http://storing.ingv.it/cfti/cfti5>, 2018.
- 714
- 715 Holland, J.H.: *Adaptation in Natural and artificial systems*, University of Michigan
716 Press, Ann Arbor, 1975.
- 717
- 718 Horvath, F., and H. Berckhemer, Mediterranean back arc basins, in *Alpine*
719 *Mediterranean Geodynamics*, pp. 145-175, eds Berckhemer, H. & Hsu, K.J.,
720 *Geodyn. Ser.*, 7, American Geophys. Un., Whashington, DC., 1982.
- 721
- 722 Jones, R.R. and Tanner, P.W.G.: Strain partitioning in transpression zones, *Journal*
723 *of Structural Geology*, 17, 793-802, 1995.
- 724
- 725 Kent, E., Boulton, S.J., Whittaker, A.C., Stewart, I.S., Cihat Alçiçek, M.: Normal fault
726 growth and linkage in the Gediz (Alaşehir) Graben, Western Turkey, revealed by
727 transient river long-profiles and slope-break knickpoints, *Earth Surface*
728 *Processes and Landforms*, 42(5), 836-52, <https://doi.org/10.1002/esp.4049>,
729 2017.
- 730
- 731 Kirby, E. and Whipple, K.X.: Expression of active tectonics in erosional
732 landscapes, *Journal of Structural Geology*, 44:54-75,
733 <https://doi.org/10.1016/j.jsg.2012.07.009>, 2012.
- 734
- 735 Lahr, J.C.: HYPOELLIPSE/Version 2.0: a computer program for determining local
736 earthquake hypocentral parameters, magnitude and first-motion pattern, U.S.
737 *Geol. Surv. Open-file Report*, 95, 89-116, 1989.
- 738
- 739 Locardi, E., Lombardi, G., Funiciello, R., Parotto, M.: The Main volcanic groups of
740 Latium (Italy): relations between structural evolution and petrogenesis,
741 *Geologica Romana*, 15, 279-300, 1977.

- 742
743 Lucente, F.P., and F. Speranza, Belt bending driven by lateral bending of
744 subducting lithospheric slab: geophysical evidences from the northern
745 Apennines (Italy), *Tectonophysics*, 337, 53-64, 2001.
746
- 747 Macka, Z: Structural control on drainage network orientation an example from
748 the Loucka drainage basin, SE margin of the Bohemian Massif (S Moravia, Czech
749 Rep.), *Landform Analysis*, 4, 109-117, 2003.
750
- 751 Malinverno, A. and Ryan, W.B.F.: Extension in the Tyrrhenian sea and shortening
752 in the Apennines as results of arc migration driven by sinking of the lithosphere,
753 *Tectonics*, 5: 227-245, 1986.
754
- 755 Mariucci, M.T., A. Amato, and P. Montone, Recent tectonic evolution and present
756 stress in the Northern Apennines (Italy), *Tectonics*, 18, 108-118, 1999.
757
- 758 Marra, F.: Low-magnitude earthquakes in Rome: structural interpretation and
759 implications for local stress-field, *Geophysical Journal International*, 138, 231-
760 243, 1999.
761
- 762 Marra, F., Strike-slip faulting and block rotation: A possible triggering
763 mechanism for lava flows in the Alban Hills? *J. Struct. Geol.*, 23 (2), 129-141,
764 2001.
765
- 766 Marra, F., Taddeucci, J., Freda, C., Marzocchi, W., Scarlato, P.: Recurrence of
767 volcanic activity along the Roman Comagmatic Province (Tyrrhenian margin of
768 Italy) and its tectonic significance, *Tectonics*, 23, TC4013.
769 doi:10.1029/2003TC001600, 2004.
770
- 771 Marra, F., Montone, P., Pirro, M., Boschi, E.: Evidence of Active Tectonics on a
772 Roman Aqueduct System (II-III Century A.D.) near Rome, Italy, *Journal of Structural*
773 *Geology*, 26, 679-690, 2004.
774
- 775 Marra F., D.B. Karner, C. Freda, M. Gaeta, and P.R. Renne, Large mafic eruptions at
776 the Alban Hills Volcanic District (Central Italy): chronostratigraphy, petrography
777 and eruptive behavior, *J. Volc. Geoth. Res.* (in press),
778 doi:10.1016/j.jvolgeores.2008.11.009, 2009.
779
- 780 Marra, F., Sottili, G., Gaeta, M., Giaccio, B., Jicha, B., Masotta M., Palladino, D.: Major
781 explosive activity in the Sabatini Volcanic District (central Italy) over the 800-
782 390 ka interval: geochronological - geochemical overview and
783 tephrostratigraphic implications, *Quaternary Science Reviews*, 94, 74-101,
784 DOI:10.1016/j.quascirev.2014.04.010, 2014.
785
- 786 Marra, F., Florindo, F., Anzidei, M., Sepe, V.: Paleo-surfaces of glacio-eustatically
787 forced aggradational successions in the coastal area of Rome: assessing interplay
788 between tectonics and sea-level during the last ten interglacials, *Quaternary*
789 *Science Review*, 148: 85-100,
790 <http://dx.doi.org/10.1016/j.quascirev.2016.07.003>, 2016.

- 791
792 Molin, D. and Rossi, A.: Effetti prodotti in Roma dai terremoti del 1703, in
793 Settecento abruzzese, in: Eventi sismici, mutamenti economico-sociali e ricerca
794 storiografica, edited by Colapietra, R., Marinangeli, G., Muzzi, P., L'Aquila, 69-106,
795 2004.
796
- 797 Montone, P, Amato A, Chiarabba C, Buonasorte G, Fiordelisi A., Evidence of active
798 extension in Quaternary volcanoes of Central Italy from breakout analysis and
799 seismicity, *Geophysical Research Letters* 1995;22: 1909-1912.
800
- 801 Montone, P. and Mariucci, M.T.: The new release of the Italian contemporary
802 stress map, *Geophysical Journal International*, 205(3),1525-1531,
803 doi:10.1093/gji/ggw100, 2016.
804
- 805 Patacca, E., and P. Scandone, Post-Tortonian mountain building in the Apennines.
806 The role of the passive sinking of a relic lithospheric slab, in *The Lithosphere in*
807 *Italy*, edited by A. Boriani, M. Bonafede, G.B. Piccardo & G.B. Vai, *Advances in*
808 *Earth Science Research. It. Nat. Comm. Int. Lith. Progr., Mid-term Conf. (Rome, 5-*
809 *6 May 1987), Atti Conv. Lincei, 80, 157-176, 1989.*
810
- 811 Patacca, E., Sartori, R., Scandone, P.: Tyrrhenian basin and apenninic arcs:
812 Kinematic relations since late Tortonian times, *Mem. Soc. Geol. Ital.*, 45, 425-451,
813 1990.
814
- 815 Parotto, M. and Praturlon, A.: Geological summary of the Central Apennines, in:
816 *Structural Model of Italy*, edited by Ogniben, L., Parotto, M., Praturlon A., *Quad.*
817 *Ric. Scient.*, 90, 257-311, 1975.
818
- 819 Pavano, F., Pazzaglia, F.J., Catalano, S.: Knickpoints as geomorphic markers of
820 active tectonics: A case study from northeastern Sicily (southern Italy),
821 *Lithosphere*, 8(6), 633-48, doi: 10.1130/L577.1, 2016.
822
- 823 Peccerillo, A.: *Cenozoic Volcanism in the Tyrrhenian Sea Region*, S. IAVCEI,
824 Barcelona, Springer, 2017.
825
- 826 Reasenberg, P. and Oppenheimer, D.: FPFIT, FPLOT and FPPAGE: FORTRAN
827 computer programs for calculating and displaying earthquake fault plane
828 solutions, USGS Open-file Report, 85-739, 1985.
829
- 830 Reutter, K.J., P. Giese, and H. Closs, Lithospheric split in the descending plate:
831 observation from the Northern apennines, *Tectonophysics*, 64, T1-T9, 1980.
832
- 833 Rovida, A., Locati, M., Camassi, R., Lolli, B., Gasperini, P.: The Italian earthquake
834 catalogue CPTI15. *Bulletin of Earthquake Engineering*, 18, 2953-2984.
835 <https://link.springer.com/article/10.1007/s10518-020-00818-y>, 2020.
836
- 837 Sambridge, M and Gallagher, K.: Earthquake hypocenter location using genetic
838 algorithms, *Bull. Seism. Soc. Am.*, 83(5), 1467-1491, 1993.
839

- 840 Selvaggi, G., and A. Amato, Subcrustal earthquakes in the Northern Apennines
841 (Italy): evidence for a still active subduction? *Geoph. Res. Lett.*, 19, 2127-2130,
842 1992.
843
- 844 Serri, G., Neogene-Quaternary magmatic activity and its geodynamic implications
845 in the Central Mediterranean region, *Ann. Geofisica*, 3, 681-703, 1997.
846
- 847 Serri, G., F. Innocenti, and P. Manetti, Geochemical and Petrological evidence of
848 the subduction of delaminated Adriatic continental lithosphere in the genesis of
849 the Neogene-Quaternary magmatism of Central Italy, *Tectonophysics*, 223, 117-
850 147, 1993.
851
- 852 Tertulliani, A. and Riguzzi, F.: Earthquakes in Rome during the past one hundred
853 years, *Ann. Geofis.*, 38, 591-606, 1995.
- 854 Tertulliani A, Graziani L, Esposito A. How historical seismology can benefit from
855 bureaucracy: the case of the "Lettere Patenti" of the city of Rome in 1703. *Seism.*
856 *Res. Lett.* 2020;91, 2511-2519. <https://doi.org/10.1785/0220200046>
857
- 858 Trasatti, E., Marra, F., Polcari, M., Etiope, G., Ciotoli, G., Darrah, T., Tedesco, D.,
859 Florindo, F., Ventura, G.: Coeval uplift and subsidence reveal magma recharging
860 near Rome, *Geochemistry, Geophysics, Geosystems*.
861 DOI:10.1029/2017GC007303, 2018
862
- 863 Tveite, H.: The QGIS Line Direction Histogram Plugin,
864 <http://plugins.qgis.org/plugins/LineDirectionHistogram/>, 2015.
865
- 866 Whipple, K.X. and Tucker, G.E.: Dynamics of the stream-power river incision
867 model: Implications for height limits of mountain ranges, landscape response
868 timescales, and research needs, *Journal of Geophysical Research: Solid Earth.*,
869 104(B8),17661-74, doi: 10.1029/1999JB900120, 1999.
870
- 871 Wobus, C., Whipple, K.X., Kirby, E., Snyder, N., Johnson, J., Spyropolou, K., Crosby,
872 B., Sheehan, D.: Tectonics from topography: Procedures, promise, and pitfalls,
873 *Special Paper of the Geological Society of America*, 55-74, 2006.
874
875